


RESEARCH

Open Access



Neurexin 3 transmembrane and soluble isoform expression and splicing haplotype are associated with neuron inflammasome and Alzheimer's disease

Akitoyo Hishimoto¹, Olga Pletnikova², Doyle Lu Lang³, Juan C. Troncoso², Josephine M. Egan³ and Qing-Rong Liu^{3*} 

Abstract

Background: Synaptic damage precedes neuron death in Alzheimer's disease (AD). Neurexins, *NRXN1*, *NRXN2*, and *NRXN3*, are presynaptic adhesion molecules that specify neuron synapses and regulate neurotransmitter release. Neurexins and postsynaptic neuroligins interact with amyloid beta oligomer (A β O) deposits in damaged synapses. *NRXN3* gene variants have been associated with autism, addiction, and schizophrenia, however, not fully investigated in Alzheimer's disease. In the present study, we investigated an AD association of a 3'-splicing allele of rs8019381 that produces altered expression of transmembrane or soluble *NRXN3* isoforms.

Methods: We carried out RT-PCR (reverse transcription polymerase chain reaction), PCR-RFLP (PCR and restriction fragment length polymorphism), Sanger sequencing, and in situ hybridization (ISH) assays for *NRXN3* neuron expression and genotyping. Genetic associations were analyzed by χ^2 tests, and ISH signals were analyzed by FISH v1.0 module of Indica Labs HALO software.

Results: We previously identified a functional haplotype in the 3' region of neurexin 3 (*NRXN3*) gene that alters the expression ratios between *NRXN3* transmembrane and soluble isoforms. In this study, we found that expression and ratio of transmembrane and soluble *NRXN3* isoforms were reduced in AD postmortem brains and inversely correlated with inflammasome component *NLRP3* in AD brain regions. The splicing haplotype related to the transmembrane and soluble *NRXN3* expression was associated with AD samples with $P = 6.3 \times 10^{-5}$ (odds ratio = 2.48) and interacted with *APOE* genotypes.

Conclusions: We found that the SNP rs8019381 of *NRXN3* that is located adjacent to splicing site #5 (SS#5) interacts with the *APOE* ϵ 4 haplotype and alters *NRXN3* transmembrane or soluble isoform expression in AD postmortem cortex. Dysregulation of presynaptic *NRXN3* expression and splicing might increase neuron inflammation in AD brain.

Keywords: Alzheimer's disease, Neurexins, Endocannabinoids, Apolipoprotein E, Alternative splicing

* Correspondence: qliu@mail.nih.gov

³Lab of Clinical Investigation, NIA-NIH, 251 Bayview Blvd, Baltimore, MD 21224, USA

Full list of author information is available at the end of the article



Background

Non-familial and late-onset Alzheimer's disease (AD) is a common cause of dementia in the elderly. Emphases on classical AD neuropathological features, A β neuritic plaques (A β -NPs), neurofibrillary tangles (NFTs), and neuro-pil threads are increasingly acknowledged to be accompanied by disrupted synaptic contacts and impaired glutamatergic neurotransmission [1, 2]. While the ϵ 4 allele of apolipoprotein E (*APOE*) gene makes a large contribution to the genetic bases of interindividual differences in vulnerability to AD, the sizable genetic influences that remain after accounting for *APOE* are likely to arise from polygenic and/or rarer variants that each makes modest contributions to overall disease vulnerability.

Diffuse A β fibrillar plaques are often observed in post-mortem human brains with normal cognitive function [3–6]. Pathological A β plaque formation around synapses with A β O deposit correlates with memory loss and synapse dysfunction [7, 8]. Neurexins were discovered as α -latrotoxin (venom of black widow spider) receptors [9] and function as presynaptic cell adhesion molecules [10] that help to regulate the release of neurotransmitters, specify, and stabilize classical synapses, including the glutamatergic synapses that provide a focus for research in AD [1, 2]. Neurexin genes are among the largest genes (greater than one million base pairs) in the human genome, and the three mammalian neurexin genes *NRXN1*, *NRXN2*, and *NRXN3* each display differential splicing events that provide thousands of neurexin isoforms on a background of longer α -neurexin and shorter β -neurexin that arise from the use of alternative promoters [11]. The larger α -neurexins contain three EGF-like (epidermal growth factor) domains each of which flanked by two LNS (lamin-neurexin-sex hormone-binding globulin) domains, a single transmembrane domain, and intracellular PDZ (*PSD95-Dlg1-Zo1*) domain that interact with intrasynaptic proteins [10, 12]. Specifically, α -neurexins are coupled to presynaptic calcium channels to regulate neurotransmitter release [13] and interact with postsynaptic neuroligins, leucine-rich repeat transmembrane proteins (*LRRRTMs*), calyntenins (*CLSTN*), α -dystroglycan (*DAG1*), GABA_A-receptors (*GABRAs*), latrophilins (*ADGRLs*), cerebellin (*CBLN*)-glutamate dehydrogenase (*GLUD*) complexes, synaptic cleft secreted neurexophilins (*NXPBs*), and intracellular PDZ-binding proteins [14, 15]. Neurexins' intracellular PDZ domains can bind to *MINT1*, *MINT2*, and *CASK* proteins [16, 17] that themselves bind to and stabilize the transmembrane form of amyloid precursor protein (*APP*) [18]. *MINT1* and *MINT2* are adaptor proteins that complex with conserved motifs in *APP*'s C-terminal region to stabilize *APP* transmembrane forms and reduce secretion of pathogenic A β cleavage products [19]. It is thus even possible that *NRXNs-MINTs* interaction complexes could alter *APP*

protein processing. Soluble or secreted α -*NRXN3* is produced by including extra exon 23 with four different intra-exonal spliced sites that encode four premature stop codons that abolishes the transmembrane and intracellular PDZ domains [20, 21]. The smaller β -neurexin contains one LNS domain (no EGF domain), a transmembrane domain, and an intracellular PDZ domain. The β -neurexin acts as a brake for endocannabinoid 2-AG (2-arachidonylglycerol) synthesis that retrogradely regulates presynaptic cannabinoid receptor 1 (CB1R)-mediated depolarization-induced suppression of excitation on AMPA and NMDA receptors that are involved in excitatory postsynaptic currents (EPSCs) [22]. *APP* cleavage enzymes of α - and γ -secretases can process β -*NRXN3* into an N-terminal extracellular domain (80 kDa) and a C-terminal intracellular domain (12 kDa). The enzymatic activities are altered by several single nucleotide polymorphisms (SNPs) of γ -secretase subunit presenilin 1 (*PSENI1*) that contribute to early-onset forms of familial AD [23]. Recent data identify roles of neurexin isoforms in several complex neuropsychiatric phenotypes that include autism [24–26], addiction [20, 27, 28], and schizophrenia [29, 30].

NRXN3 mRNA is the second most reduced gene after vacuolar H⁺-ATPase subunit gene *ATP6V1E1* in AD hippocampus identified by bioinformatic analysis of AD and aging Gene Expression Omnibus (GEO) databases [31, 32]. We have identified 3' region of *NRXN3* haplotypes that are tagged by alleles of the SNP rs8019381, which is located near the end of *NRXN3*'s exon 23 at a key splicing site [20]. Alleles of rs8019381 tagged *NRXN3* produce the splice variants that include or exclude exon 23 coding for a single transmembrane domain; thus, transmembrane or soluble *NRXN3* isoforms are transcribed and translated, respectively [20]. *NRXN3* is expressed in neurons in brain regions that are implicated in mnemonic processes and in dementia-associated AD pathologies. For example, *NRXN3* is expressed in the cerebral cortex and in the hippocampus that contains AD-related senile plaques and neurofibrillary tangles [33, 34]. Differences in the properties of synapses in these regions could alter brain connectivity, and the altered ratio of transmembrane and soluble *NRXN3* isoforms could lead to pathological A β O accumulation at synapses.

We have thus characterized the patterns of expression of total *NRXN3*, α -*NRXN3* and β -*NRXN3*, and four *NRXN3* transmembrane and soluble splice variants in mRNAs extracted from postmortem middle frontal gyrus from pathologically confirmed AD and control individuals. We have sought AD-related differences in frequencies of *NRXN3* haplotypes and tested whether the *NRXN3* associations are dependent on the *APOE* genotype. Finally, we have found evidence for *NRXN3* association and interaction with *APOE* genotypes in previously

reported genome-wide association datasets and for *NRXN3* inverse correlation with inflammasome component *NLRP3* in neurons of the AD hippocampus and cortex. Taken together, these data support contributions for common human *NRXN3* haplotypes and altered *NRXN3* transmembrane and soluble isoform expression in AD brain.

Methods

Subjects: human samples

Middle frontal gyrus postmortem brain samples of 121 European-American AD (38 men and 83 women with mean age 80.3 ± 9.6) were obtained from the Division of Neuropathology, the Department of Pathology, the Johns Hopkins University School of Medicine (JHUSOMI), whose diagnoses were all confirmed by autopsy [35].

Additional European-American comparison groups comprising 349 subjects were examined to document the distribution of *NRXN3* polymorphism in the general American Caucasian population of the USA. One hundred sixty samples (107 men and 53 women with mean age 36.1 ± 16.2) were obtained from Maryland Brain Bank (UMD) whose geographical location is close to that of AD subject collection. One hundred eighty-nine unrelated subjects (42 men and 147 women with mean age 51.2 ± 14.9) were selected from pedigrees from the Collaborative Study on the Genetics of Alcoholism (COGA) [36]. We explored mRNA levels of *NRXN3* isoforms in middle frontal gyrus postmortem samples from 58 pathologically confirmed AD subjects and 48 control subjects. We also explored the association between this *NRXN3* haplotype and AD with 121 pathologically confirmed AD subjects and 349 control subjects.

RNA isolation and cDNA synthesis

Total RNA was extracted from the larger sized middle frontal gyrus samples available from 58 of the autopsy-confirmed European-American AD patients and 48 normal individuals dying without neurological disease (40 females/18 males, mean age \pm SD; 81.2 ± 10.0 , PMI; 11.4 ± 6.4 from JHMI and 11 females/37 males, mean age \pm SD; 47.6 ± 19.7 , PMI; 11.9 ± 6.0 from JHMI and

UMD) using Trizol (Thermo Fisher, Waltham, MA) protocol. Single-strand cDNA was synthesized from total RNA using SuperScript™ III One-Step RT-PCR System (Invitrogen, Carlsbad, CA, USA). Electrophoresis of all RNAs used for quantitative PCR revealed sharp 18S and 28S ribosomal RNA bands; four samples with evidence for RNA degradation were eliminated on this basis.

Quantitative RT-PCR

For quantitative real-time PCR assessments of *NRXN3* mRNAs, isoform-specific primers and minor groove-binding (MGB) TaqMan probes were designed using Primer Express Software (Table 1), common *NRXN3* TaqMan probe (Hs01028186_m1), and endogenous control glyceraldehyde-3-phosphate dehydrogenase (*GAPDH*, Vic-labeled) which were ordered from Thermo Fisher (Cat#4326317E, Thermo Fisher Scientific, Waltham, MA, USA). The relative fold change is calculated using the formula $2^{(-\Delta\Delta C_t)}$.

Genetic testing

Genomic DNA was extracted from blood or tissue samples from the individuals noted in “human samples” above. DNA from most AD and control samples was extracted from the middle frontal gyrus brain tissues using Qiagen genomic DNA kits. Genomic DNA for other subjects was extracted from peripheral leukocytes as previously described [37]. *APOE* polymorphisms were genotyped using PCR-RFLP assays as described [38]. The rs8019381 SNP was genotyped by direct Sanger sequencing as described [20].

RNAscope in situ hybridization (ISH)

Human postmortem hippocampus (1 control sample of Braak 0 and 3 AD samples of Braak 6) and middle temporal gyrus (2 control samples of each Braak 0, 1, and 2 and 2 AD samples of each Braak 4, 5, and 6) were used for triplex fluorescent ISH. Human RNAscope ISH probes were ordered from Advanced Cell Diagnostics Inc. (ACD, Hayward, CA, USA) for *NRXN3* in C2 channel (20 ZZ pairs targeted region 1095–2035 of NM_001105250.2; Cat No. 525431-C2), *NLRP3* in C1 channel (30 ZZ pairs

Table 1 Real-time PCR primers and MGB Fam-TaqMan probes for *NRXN3* isoforms

<i>NRXN3</i>	Forward primers	Reverse primers	MGB probes
Hs01028186_m1	NRXN3 TaqMan gene expression assay		
ex 22a24a	TGATCTTGTTTCATCTGCTGAATG	AAGGTGCACGAGTAGCAATAG	CCGAGTACAGGAGGTG
ex 22a24b	TGATCTTGTTTCATCTGCTGAATG	TGCTTTGTAGCCACCTTCGA	CCGAGTACAGATAAGAGTC
ex 22a24c	TGATCTTGTTTCATCTGCTGAATG	CCCGGAACCCGTCTGATT	CCGAGTACAGCAAAC
ex 22a23a	AGATGATCTTGTTTCATCTGCTGAA	CGGAGTGATCTAGCTGCATTAGAG	CCGAGTACAGCCAGAAG
ex α 1-2	GACATACAGACAGATCCCAAATCTTC	TCATGGTGCGCCAGAA	AACTGGAAGGTCTTTTC
ex β 1-18	TCCCCTGTTCCCTTCGA	GCCACCACCTTTCCCAA	AGGACACGCTGGCC

targeted region 2627–4008 of NM_004895.4; Cat No. 478021), and *NEUN/RBFOX3* in C3 channel (20 ZZ pairs target region 720–2217 of NM_001082575.2; Cat No. 415591-C3). The positive control probes (Cat No. 320868) were *POLR2A* (C1 channel), *PPIB* (C2 channel), and *UBC* (C3 channel). The negative control probe was bacterium (*Bacillus subtilis*) gene *DapB* (Cat No. 320871). The cryostat sectioning of postmortem human brain samples, fixation, protease pretreatment, probe hybridization, pre-amplification, amplification, horseradish peroxidase reaction, and fluorescent labeling steps were described previously [39]. Zeiss LSM 880 confocal microscope was used to image fluorescent labeling. Amplification $\times 20$ images (two to three images for each brain sample) were analyzed by FISH v1.0 module included in HALO software with RNAscope ISH setting (Indica Labs, Corrales, NM, USA). The H-score [$\sum_{\text{bin}0-4}$ (ACD score or bin number \times percentage of cells per bin)] were used to calculate mRNA expression for each probe based on the minimum intensity threshold (a value between 0 and 400).

Statistical analysis

Genetic associations were analyzed by χ^2 tests. Deviations from Hardy-Weinberg equilibrium (HWE) were examined by χ^2 test with $P < 0.05$ as a deviation from HWE. Correction for multiple testing was not applied because of the a priori reason to focus on rs8019381 in this study. Power analyses used the program PS v2.1.31 [40]. Comparison of the ages in AD between the rs8019381 SNP genotype groups was analyzed using ANOVA. Logistic regression analysis was also applied using phenotype as the dependent variable, and the age, gender, APOE $\epsilon 4$ allele, and rs8019381 genotypes as the independent variables. Statistical analyses of mRNA expression RT-PCR and ISH data were performed using PRISM (GraphPad Software, CA, USA) software. Differences in the mRNA expression levels based on phenotype (control vs AD or genotype CC vs CT and TT) were examined using two-tailed Mann-Whitney tests. Two-way ANOVA and two-tailed/unpaired Student's *t* test using H-scores of ISH intensities were tested for any significant differences between *NRXN3* and *NLRP3* expressions in different Braak stages of MTG and HIP samples. Linear regression of H-scores of each ISH probe was used to fit straight lines through control and AD data sets with different Braak staining stages and statistically calculated for any significant differences. $P < 0.05$ was considered significant for comparisons of expression levels. Spearman's rank correlation coefficient analyses were used to assess the contributions of age, sex, and postmortem interval to the mRNA expression levels of each splice variant.

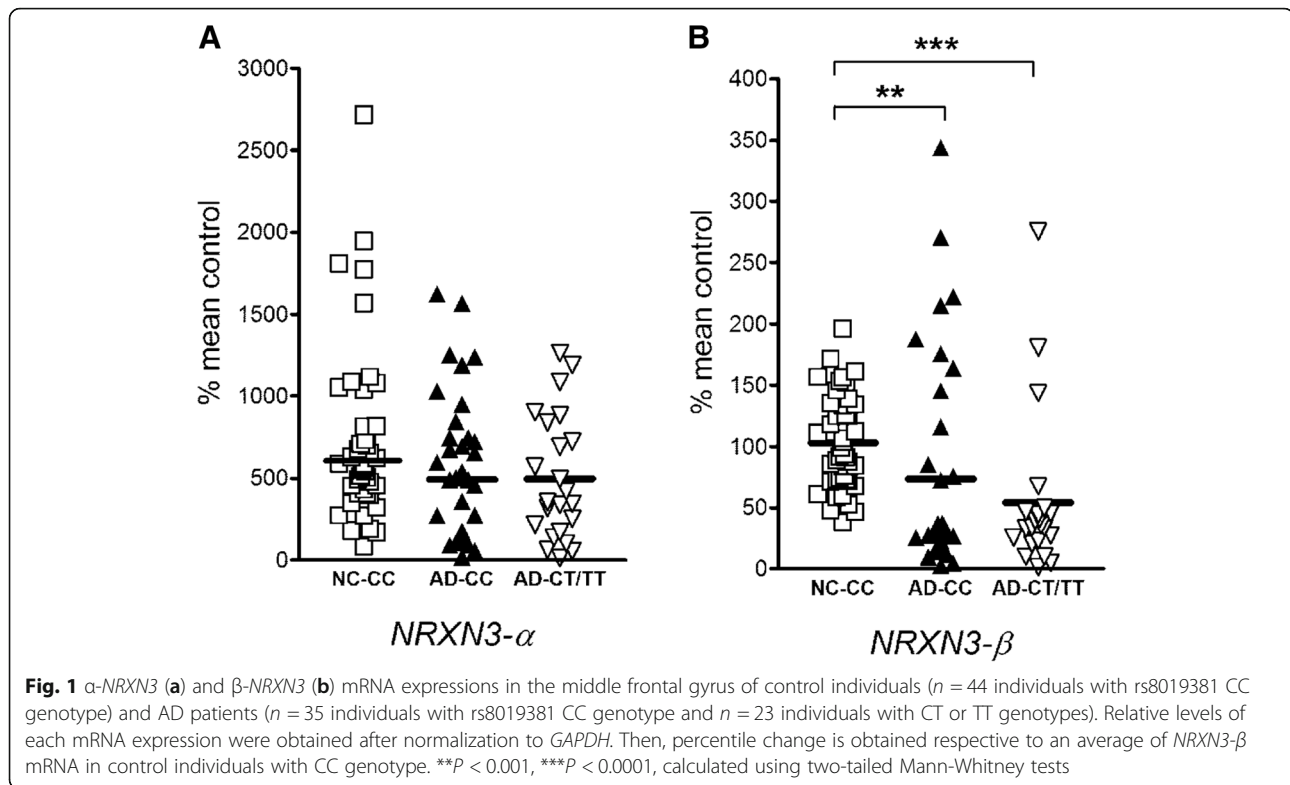
Results

α -*NRXN3* and β -*NRXN3* mRNA expression in AD middle frontal gyrus

We compared expression of α -*NRXN3* and β -*NRXN3* in mRNAs extracted from the middle frontal cortices of human postmortem brain samples of AD and controls with different “splicing site 5 (SS#5)” *NRXN3* haplotypes defined by alleles of the rs8019381 SNP. Since controls displayed few rs8019381 T alleles, we compared control samples with CC genotypes to AD samples with CC genotype and to AD samples with either one or two T alleles (CT/TT). There were no significant differences between expression of α -*NRXN3* mRNA in CC controls vs AD patients with either CC or CT/TT genotypes (Fig. 1a; two-tailed Mann-Whitney $P = 0.067$ and $P = 0.127$, respectively). By contrast, when compared with control individuals with CC genotypes, β -*NRXN3* mRNA expression levels decreased by 30% and 48% in AD patients with CC and CT/TT genotypes, respectively (Fig. 1b; $P = 0.0004$ and $P < 0.0001$, respectively). We identified a mild significant correlation between age and either α -*NRXN3* or β -*NRXN3* mRNA expression levels in the combined groups (Fig. 2a; $P = 0.0473$, Spearman $r = 0.193$ and $P = 0.0061$, Spearman $r = 0.2648$, respectively). However, we identified neither a trend nor a significant correlation between age and either α -*NRXN3* or β -*NRXN3* mRNA expression levels in the control groups (Fig. 2b; $P = 0.787$, Spearman $r = 0.040$ and $P = 0.386$, Spearman $r = 0.128$, respectively). We also did not identify significant correlations between α -*NRXN3* and β -*NRXN3* mRNA expression levels in the AD group and age (Fig. 2c; $P = 0.253$, Spearman $r = 0.153$ and $P = 0.186$, Spearman $r = 0.176$, respectively). In these AD samples, the positive slope of this regression line does indicate trends toward less *NRXN3* expression in older individuals with AD phenotype. Neither gender nor postmortem intervals were correlated with these expression levels in control or AD groups (data not shown). In the AD subjects, there were no differences in expression of either α -*NRXN3* ($P = 0.751$) nor β -*NRXN3* isoforms ($P = 0.863$) in individuals with haplotypes marked by CC vs CT/TT genotypes.

Genetic analysis

Table 2 shows the genotype distribution and allele frequency of rs8019381 SNP for AD and control groups. The genotype distributions differed remarkably between the AD and control groups ($\chi^2 = 15.587$, $df = 2$, $P = 0.000413$). The minor allele frequency of the rs8019381 T allele was significantly greater for the AD group than for the control group (0.157:0.070, respectively; $\chi^2 = 15.997$, $df = 1$, $P = 0.0000634$). These results correspond to an odds ratio of 2.48 (95% confidence intervals 1.57–3.91) for AD in individuals with this T allele. Based on the observed allele frequency of the



rs8019381 SNP, the current samples yielded the power of 0.894 for detecting nominally significant results. There was no significant effect of age on the distribution of rs8019381 genotypes in the AD group ($P = 0.562$ by one-way ANOVA). The rs8019381 genotype distributions also displayed no significant deviation from Hardy-Weinberg equilibrium in either the AD or control groups (data not shown).

We next investigated the *APOE* genotypes in these samples and sought possible interactions with the effects of the *NRXN3* haplotypes marked by the rs8019381 SNP (Table 2). As expected, the *APOE* genotype and allele frequency distributions of the AD samples differed significantly from those of the control group ($\chi^2 = 87.146$, $df = 5$, $P = 2.671 \times 10^{-17}$ and $\chi^2 = 92.374$, $df = 2$, $P = 8.735 \times 10^{-21}$, respectively; Table 2).

When we sought interactions between the rs8019381 SNP and *APOE* genotypes in the AD group, the rs8019381 genotype distributions displayed significant differences between *APOE* $\epsilon 4$ non-carriers and *APOE* $\epsilon 4$ carriers ($\chi^2 = 8.043$, $df = 2$, $P = 0.0179$). Among AD individuals, rs8019381 TT homozygotes were found only in those who did not carry *APOE* $\epsilon 4$ alleles. This difference provided significance for recessive analysis (comparing CC + CT vs TT) of the differences between AD *APOE* $\epsilon 4$ non-carriers and AD *APOE* $\epsilon 4$ carriers ($\chi^2 = 6.317$, $df = 1$, $P = 0.012$), though not for analyses of allele frequencies ($\chi^2 = 0.429$, $df = 1$, $P = 0.513$). These results

contrasted with those in control samples, where we found that neither genotype distributions nor allele frequencies were significantly different between *APOE* $\epsilon 4$ non-carriers and *APOE* $\epsilon 4$ carriers ($P = 0.428$ and 0.541 for genotype and allele comparisons, respectively).

Overall, significant associations between the rs8019381 genotypes and AD thus remained in both *APOE* $\epsilon 4$ non-carriers ($P = 0.000403$) and in *APOE* $\epsilon 4$ carriers ($P = 0.00331$). The allele frequencies for the rs8019381 SNP also differed significantly in AD vs control comparisons in both the *APOE* $\epsilon 4$ non-carriers ($P = 0.00252$) and *APOE* $\epsilon 4$ carriers ($P = 0.00827$). We also confirmed a significant effect of rs8019381 polymorphism on the AD phenotype considering for age, gender, and *APOE* $\epsilon 4$ allele ($P = 0.00157$, Table 3).

As anticipated for loci on distinct chromosomes, *APOE* (19q13) and *NRXN3* (14q24) markers displayed evidence for independent segregation in these samples. Neither the genotype distribution nor allele frequency of rs8019381 SNP was associated with the *APOE* allele frequency among the AD or control groups ($P_{AD} = 0.061$, $P_{CTL} = 0.850$ and $P_{AD} = 0.600$, $P_{CTL} = 0.283$ for genotypic and allelic comparisons, respectively).

Genetic variation and *NRXN3* SS#5 splice variants in AD

Since the *NRXN3* haplotype tagged by rs8019381 (Fig. 3a) has been associated with altered patterns of expression of *NRXN3* splice variants that encode

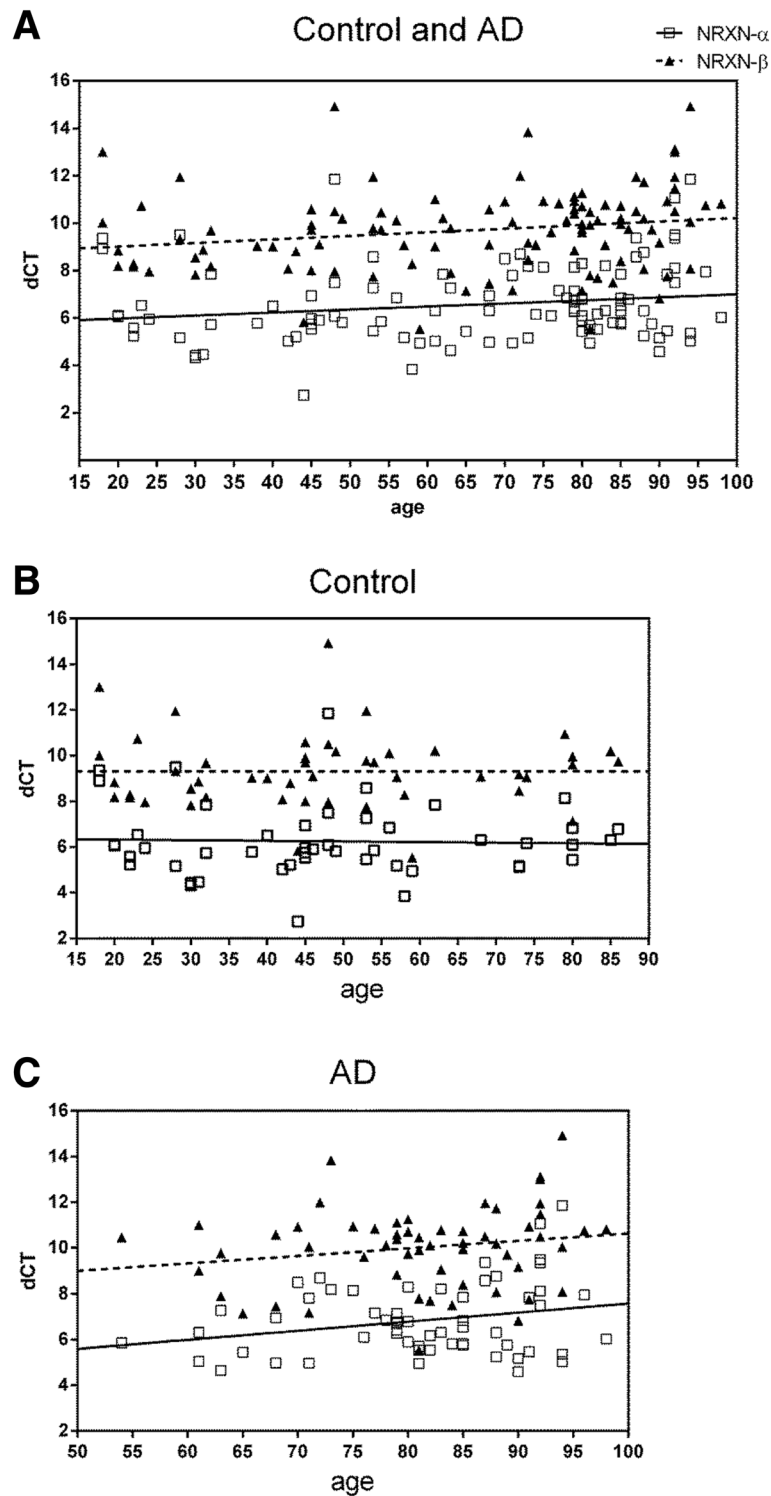


Fig. 2 **a** Correlation between age and either α -NRXN3 or β -NRXN3 mRNA expression levels in the control and AD combined groups ($P = 0.0473$, Spearman $r = 0.193$ and $P = 0.0061$, Spearman $r = 0.2648$, respectively). **b** Correlation between α -NRXN3 and β -NRXN3 mRNA expression levels in the control group and age ($P = 0.787$, Spearman $r = 0.040$ and $p = 0.386$, Spearman $r = 0.128$, respectively), and **c** in the AD group and age ($P = 0.253$, Spearman $r = 0.153$ and $P = 0.186$, Spearman $r = 0.176$, respectively). ΔC_t values of each isoform expression were obtained after normalization to C_t values of *GAPDH*

Table 2 Distribution of the *NRXN3* rs8019381 C/T SNP and *APOE* allele frequencies among the rs8019381 genotypes

Group	Genotype ^a			Allele frequency		P value	
	CC	CT	TT	C	T		
rs8019381 genotype and allele frequencies ^b							
Control (n = 336)	291 (0.866)	43 (0.128)	2 (0.006)	0.930	0.070	Genotype: $P = 0.00041$ ($\chi^2 = 15.6$, $df = 2$) Allele: $P = 0.000063$ ($\chi^2 = 16.0$, $df = 1$)	
AD (n = 121)	86 (0.711)	32 (0.264)	3 (0.025)	0.843	0.157		
rs8019381 genotypes among <i>APOE</i> $\epsilon 4$ non-carriers and <i>APOE</i> $\epsilon 4$ carriers							
Control	<i>APOE</i> $\epsilon 4$ non-carriers	216 (0.857)	35 (0.139)	1 (0.004)	0.927	<i>APOE</i> $\epsilon 4$ non-carriers VS. $\epsilon 4$ carriers in the AD Genotype: $P = 0.018$ ($\chi^2 = 8.0$, $df = 2$) Allele: $P = 0.000063$ ($\chi^2 = 0.43$, $df = 1$)	
	<i>APOE</i> $\epsilon 4$ carriers	75 (0.893)	8 (0.095)	1 (0.012)	0.940		0.060
AD	<i>APOE</i> $\epsilon 4$ non-carriers	26 (0.722)	7 (0.195)	3 (0.083)	0.819		0.181
	<i>APOE</i> $\epsilon 4$ carriers	60 (0.706)	25 (0.294)	0 (0.000)	0.853		0.147

^aNumber of subjects (frequency)

^brs8019381: Significant differences were found between the AD and the controls in either the genotype distribution ($\chi^2 = 15.587$, $df = 2$, $P = 0.000413$) or the allele frequencies ($\chi^2 = 15.997$, $df = 1$, $P = 0.0000634$)

transmembrane vs soluble isoforms, we evaluated the distributions of these isoforms in control brains, which were virtually all from individuals with CC haplotypes, and in frontal cortex samples of AD brains from CC, CT, and TT individuals. We have previously noted that the predominant *NRXN3* transmembrane isoforms that arise from alternative splicing at SS#5 are exon 22a-24b, exon 22a-24c, and exon 22a-24a, while the predominant soluble isoform comes from exon 22a-23a-24a. We thus assessed the levels of these four isoforms (Fig. 3b).

The most prominent result of these assays, as with studies of total *NRXN3*, α -*NRXN3*, and β -*NRXN3* mRNA levels, was the reduced expression that was found for most of the isoforms in the AD postmortem middle frontal gyrus (MFG), middle temporal gyrus (MTG), and hippocampus (HIP) (Fig. 3c). In comparison with one-half reduction of total *NRXN3* expression in the AD cortex, the exon 22a-24b variant that encodes the major transmembrane isoform was expressed at levels that were decreased, by 85% in AD subjects with either CC or CC/TT genotypes ($P < 0.0001$ by two-tailed Mann-Whitney tests for both comparisons) (Fig. 4b). Levels of the exon 22a-24c variant, the second major transmembrane isoform were also decreased by 56% and

66% in AD patients with CC and with CC/TT genotypes when compared with control CC individuals (Fig. 4c; $P < 0.0001$ by two-tailed Mann-Whitney test for both comparisons). Overall differences in mRNA expression levels for these two transmembrane isoforms between CC and CT/TT genotypes were not detected among the AD patients ($P = 0.611$ and 0.476 by two-tailed Mann-Whitney tests, respectively).

The major soluble *NRXN3* isoform, encoded by the exon 22a-23a variant mRNA was also decreased by 63% and 71% in AD patients with CC and CC/TT genotypes when compared with those in control individuals with CC genotypes (Fig. 4d; $P < 0.0001$ by two-tailed Mann-Whitney test for both comparisons). Differences in mRNA expression levels between CC and CT/TT genotypes were not detected among the AD brains ($P = 0.455$ by two-tailed Mann-Whitney test).

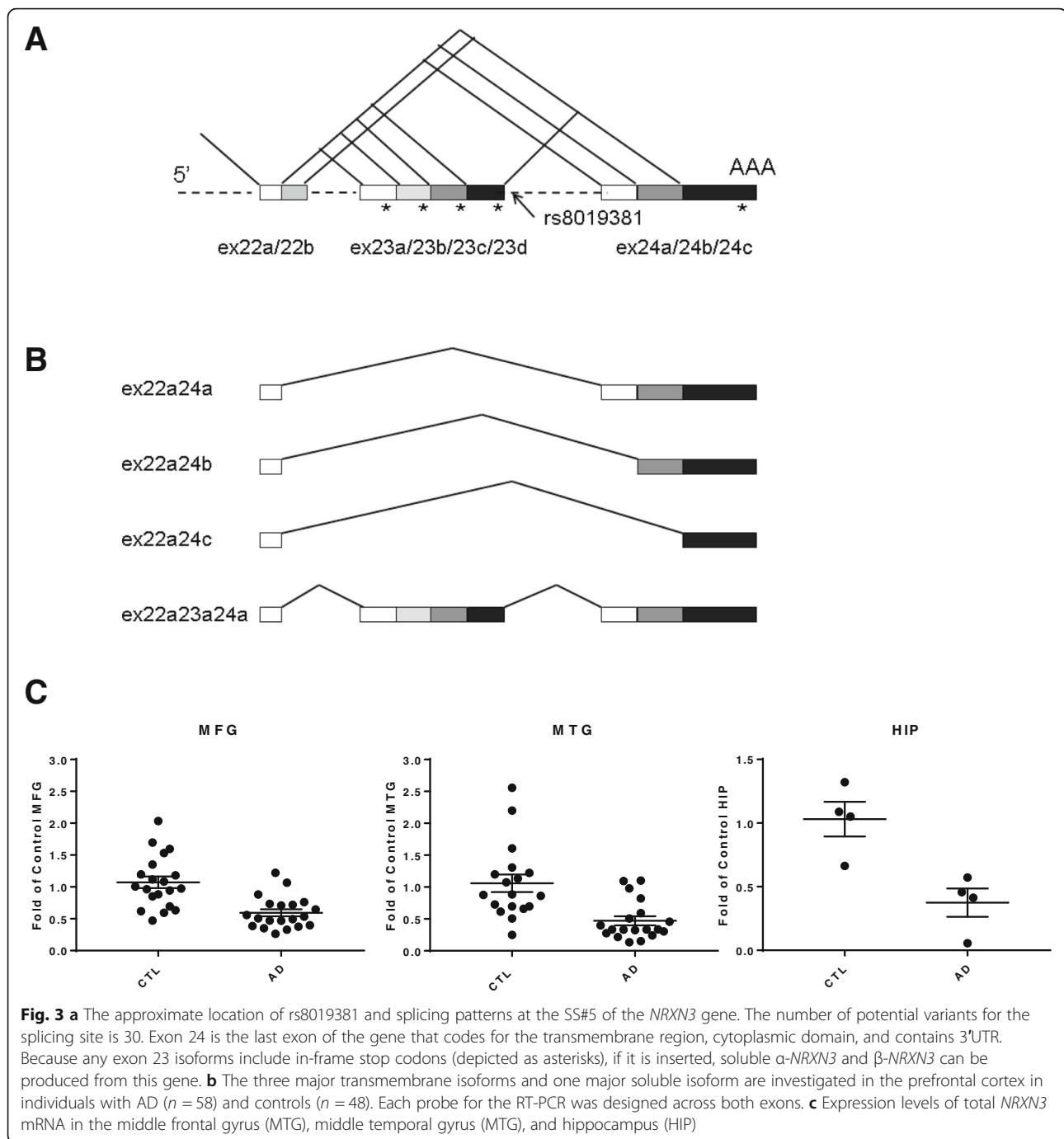
Closer examination revealed evidence for interactions between the clinical phenotype, the AD susceptible rs8019381 T allele, and expression of the exon 22a-24a mRNA that encodes a major transmembrane isoform (Fig. 4a). Expression of exon 22a-24a mRNA was decreased by 46% in AD patients with CT/TT genotypes when compared with those in control individuals with CC genotypes ($P = 0.0002$, two-tailed Mann-Whitney tests). Within the AD group, exon 22a-24a mRNA expression levels were also decreased by 46% in AD patients with CT/TT genotypes when compared with those with CC genotypes ($P = 0.043$ by two-tailed Mann-Whitney tests). By contrast, exon 22a-24a mRNA expression levels did not differ significantly between control and AD samples with CC genotypes ($P = 0.180$ by two-tailed Mann-Whitney test). These differences correlated with differences in the ratios between transmembrane and soluble isoform expression in CC vs CT/TT AD individuals, and the ratio differences reached the margin of statistical significance (Fig. 5). In AD patients, the ratios of transmembrane vs soluble

Table 3 Logistic regression analysis of rs8019381 C/T SNP on the AD phenotype considering for age, gender, and *APOE* $\epsilon 4$ allele

Coefficients of bias-reduced logistic regression				
Variable	Parameter	Standard error	Wald χ^2	P value
Intercept	-13.917	1.528	-9.107	<0.0001
Age	0.179	0.020	8.750	<0.0001
Gender	-0.051	0.416	-0.123	0.902
<i>APOE</i> $\epsilon 4$ allele ^a	1.691	0.403268658	4.194	0.000033
rs8019381 genotype ^b	3.078	0.968	3.181	0.00157

^aFor *APOE* $\epsilon 4$ allele analyses, $\epsilon 4$ non-carriers were coded as 0 and *APOE* $\epsilon 4$ carriers were coded as 1

^bFor rs8019381 genotype analyses, each SNP was coded as 0 for major allele homozygotes, 0.5 for heterozygotes, and 1 for minor allele homozygotes



isoforms were 25% greater in CT/TT than in CC subjects ($P = 0.053$ by two-tailed Mann-Whitney test and $P = 0.044$ by unpaired t test) despite that the overall ratio of the transmembrane and soluble isoforms decreased in AD brains. Interestingly, these ratios did not differ between AD patients with CT/TT genotypes vs those in control CC individuals ($P = 0.331$ by two-tailed Mann-Whitney tests).

Inverse correlation of *NRXN3* with inflammasome component *NLRP3* in AD brains

We carried out an ultra-sensitive RNAscope ISH assay to study the altered *NRXN3* expression at cellular levels in control and AD postmortem brain samples that were co-hybridized and co-stained with inflammasome component *NLRP3* [41] and neuron marker *NEUN/RBFOX3*. All *NRXN3* and the majority of *NLRP3* signals were

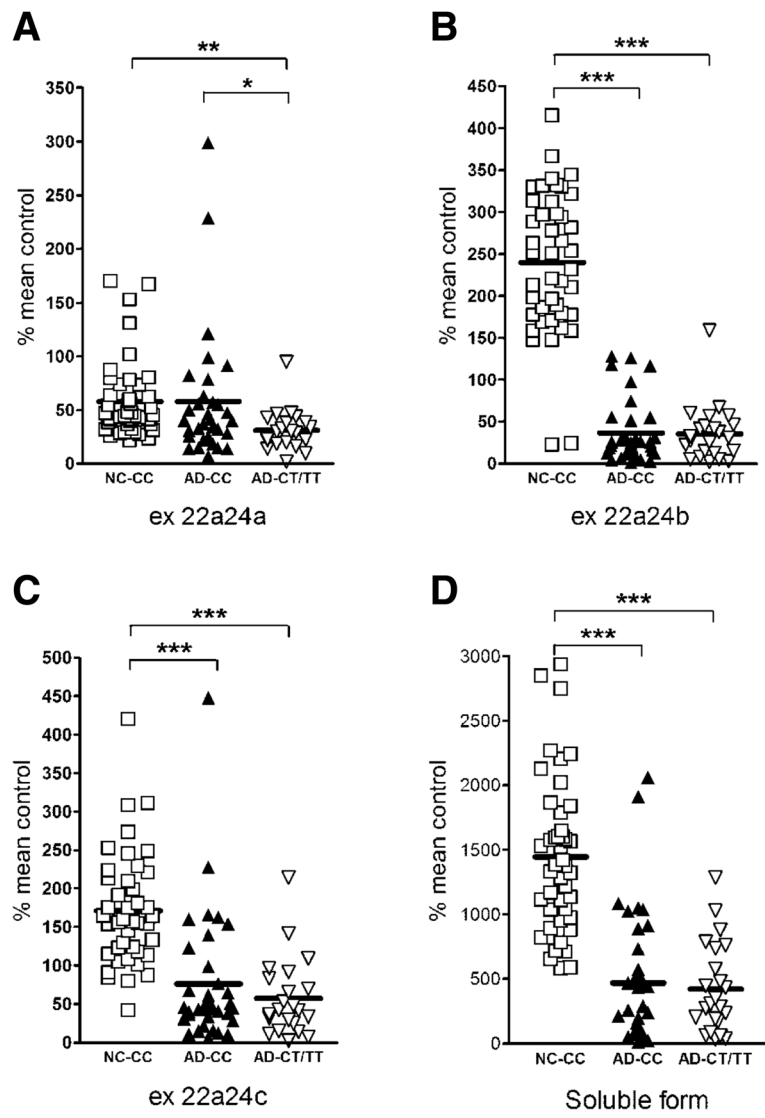
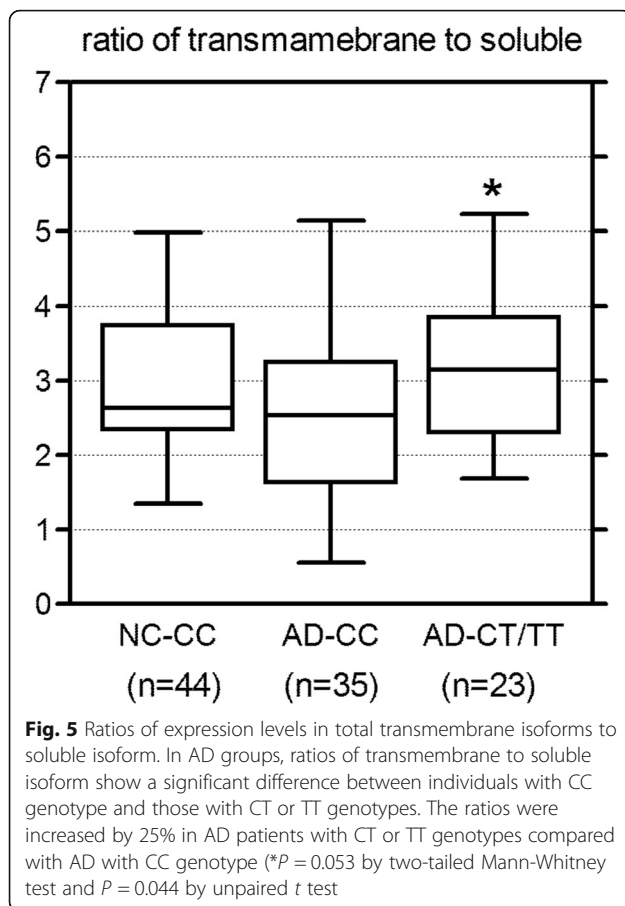


Fig. 4 a-c Expression levels of mRNAs encoding *NRXN3* transmembrane isoforms (exon 22a-24a, exon 22a-24b, and exon 22a-24c variants, respectively) and **d** *NRXN3* soluble isoform (exon 22a-23a variant) in the middle frontal gyrus of control individuals ($n = 44$ individuals with rs8019381 CC genotype) and AD patients ($n = 35$ individuals with rs8019381 CC genotype and $n = 23$ individuals with CT or TT genotypes). Relative levels of each mRNA expression were obtained after normalization to GAPDH. Then, percentile change is obtained respective to an average of β -*NRXN3* mRNA in control individuals with CC genotype. * $P < 0.05$, ** $P < 0.001$, *** $P < 0.0001$, calculated using two-tailed Mann-Whitney tests

co-localized with *NEUN/RBFOX3*-positive neurons (Fig. 6). We found that the reduced *NRXN3* mRNA was inversely correlated with the increased *NLRP3* mRNA in *NEUN/RBFOX3*-positive neurons of the AD middle temporal gyrus (Fig. 6a-f) and hippocampus (Fig. 6g, h) samples. Two-tailed and unpaired Student's *t* test using H-scores that represent *NRXN3* neuron expression was significantly higher than that of *NLRP3* at Braak 2 stage of MTG and significantly lower at Braak 6 stage in MTG and HIP (Fig. 7a). Two-way ANOVA analysis found significant differences of H-scores in HIP ($F_{1,14} = 6.07$; $P = 0.0273$) but not in MTG ($F_{1,28} = 0.45$; $P = 0.4515$)

with different Braak stages; however, the interaction of *NRXN3* and *NLRP3* neuron expression in MTG and HIP at different Braak stages were very significant ($P < 0.0001$). Linear regression analysis using H-score for each Braak number (0, 1, 2, 4, 5, 6) found that the differences of slopes of *NRXN3* and *NLRP3* were significant ($F_{1,8} = 11.49$; $P = 0.0095$) in MTG samples. *NLRP3* regression slope was significantly non-zero ($F_{1,4} = 18.32$; $P = 0.0128$), and *NRXN3* regression slope was not significantly non-zero ($F_{1,4} = 0.98$; $P = 0.3773$). The correlation was also simulated in control (Braak = 0) and AD (Braak = 6) in HIP samples. The linear regression lines for *NRXN3* and



NLRP3 intersected at 2.6 and 2.1 Braak grades in MTG and HIP samples, respectively (Fig. 7b). We did not observe any significant correlation of *NEUN/RBFOX3* with Braak stages (data not shown).

Discussion

We found that *NRXN3* gene haplotype interacts with the *APOE* $\epsilon 4$ haplotype, and the expression and ratio of its transmembrane and soluble isoforms were reduced in AD postmortem MFG. *NRXN3* mRNA level was inversely correlated with that of inflammasome component *NLRP3* in MTG AD neurons. The linear regression of *NRXN3* and *NLRP3* signals that intersected at Braak 2.1 for HIP and Braak 2.6 for MTG might indicate differential progression of A β fibrils in different brain regions. Previous studies by array tomography and electron microscopy find that A β O forms halo at synapses that attracts A β fibrils around damaged neurites [42–44]. The most prominent AD-associated susceptible genes and their altered expression/splicing/translation/PTM (posttranslational modifications), such as *APP* and *PSEN1* [23, 45], *APOE* and *APOER2* [46], *PTK2B* [47], *PPP3CA* and *PPP3R1* [48, 49], and *PINI* [50], are involved in synaptic homeostasis. Dysregulation of

presynaptic *NRXN3* might be an early event that triggers synaptic calcium dyshomeostasis and let A β O invasion at synapses. Subsequent dystrophic neurites and dysfunctional synapses stimulate *NLRP3*/caspase-1 and calcineurin/caspase-3 pathways that activate interleukin-1 β and interleukin-18 [51, 52] and cause mitochondria impairment and apoptosis [53], respectively. A β fibrils are at their peak when AD symptom just appears [54], and *NRXN3* and *NLRP3* expression trajectories might serve as early diagnosis and therapeutic targets at early Braak 2–3 stages.

NRXN3 SNP rs8019381 was found to contribute to AD susceptibility. There is no information available for rs8019381 in previously reported genome-wide association studies for AD [3, 55, 56] because of the relatively small haplotype block (14 kb) in the study. While no genomic markers that display strong linkage disequilibrium with rs8019381 are identified in the Translational Genomic Research Institute (TGen) datasets [56], we identified rs2067730 that lies about 6 kb 5' to rs8019381 in genome-wide association studies of clinically diagnosed AD vs control subjects of European ancestries who were recruited from Canadian memory clinics [55]. Interestingly, like *NRXN3* rs801938, rs2067730 displays association with AD in this sample and appears to interact with the *APOE* genotype ($P = 0.027$).

The magnitude of rs8019381 association suggests an odds ratio of 2.48, with a broad 95% confidence interval that encompasses 1.6–3.9. While this effect is much less than the large, oligogenic influence of *APOE* haplotypes on AD vulnerability, it is larger than many of the effects of other proposed polygenic variants listed in systematic meta-analysis presented on the AlzGene database [57] or in two genome-wide association datasets that compare AD vs control samples [3, 55, 56]. The effects of the *NRXN3* haplotype may be even larger in individuals with specific *APOE* haplotypes. Both the current dataset and data reported by Li et al [55] provide evidence for significant interactions among *APOE* haplotypes and 3' *NRXN3* haplotypes in AD.

The reduced expression of total *NRXN3*, α -*NRXN3*, and β -*NRXN3* in samples of the cerebral cortex and hippocampus from pathologically confirmed AD and control brains formed the initial basis for implicating *NRXN3* in AD. These findings were accompanied by a significant reduction of ratios between transmembrane and soluble isoforms in AD individuals with rs8019381 CT or TT genotypes. These observations support the hypothesis that reduction of *NRXN3* transmembrane isoform alters synapse homeostasis, reduces neurotransmitter release, and promotes A β oligomerization and *APOE* dysfunction in synaptic degeneration [7, 58]. Alternatively, the altered ratio might differentially interact with alternatively spliced isoforms of *APP*, causing increased A β production [59].

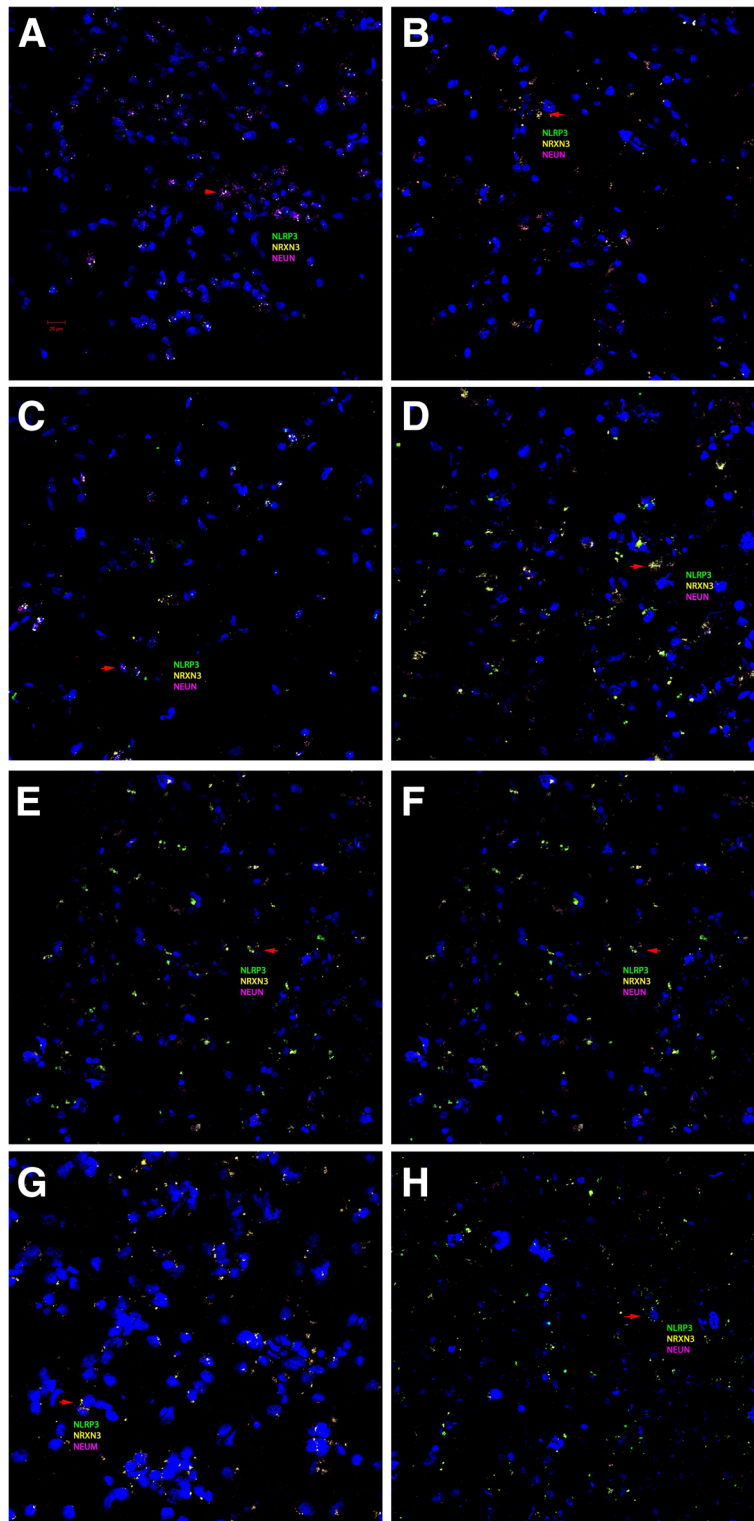
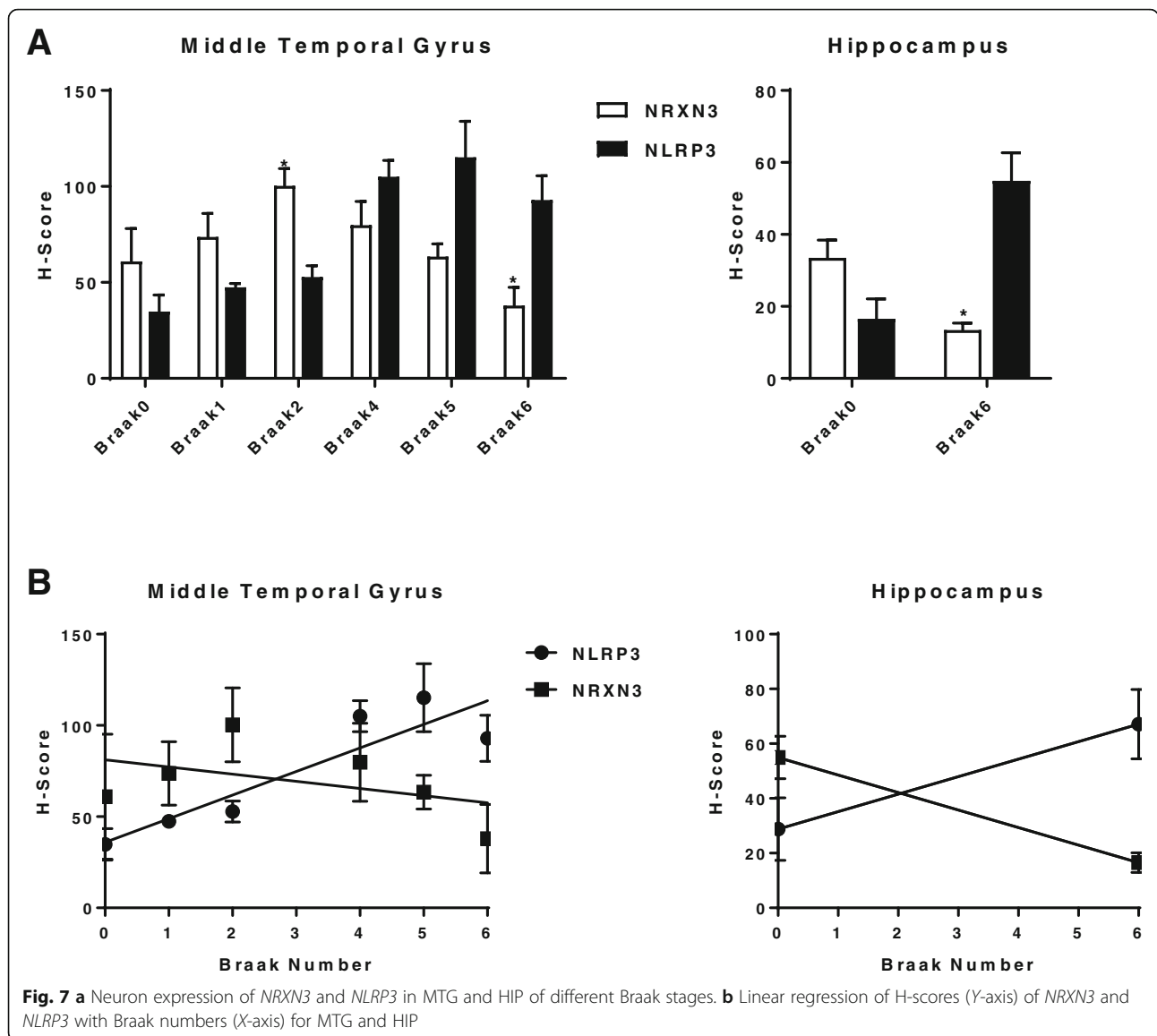


Fig. 6 a–h RNAscope in situ hybridization of control and AD brain samples with different Braak numbers. Green represents *NLRP3*, yellow *NRXN3*, and magenta *NEUN*. The red arrow indicates colocalization of three probes in the same cell. H-score correlations of *NRXN3* and *NLRP3* intensities with Braak numbers. **(a)** MTG-Braak 0; **(b)** MTG-Braak 1; **(c)** MTG-Braak 2; **(d)** MTG-Braak 4; **(e)** MTG-Braak 5; **(f)** MTG-Braak 6; **(g)** HIP-Braak 0; **(h)** HIP-Braak 6



The associated *NRXN3* SNP rs8019381 is located at the junction of exon 23's splicing donor site (23 base pairs downstream from the 3' of exon 23), within a region that might alter splicing efficiency. The *NRXN3* haplotype studied here is likely to be different from other ethnic samples. The rs8019381 "T" allele frequency (0.07) of the control samples reported here (based on genotypes from 672 chromosomes) is similar to values obtained in unselected Europeans and European-Americans available (0.094 based on genotypes from 224 chromosomes) from dbSNP. African Yoruban rs8019381 frequency (0.198) is (based on genotypes of 180 chromosomes) higher than European population, and East Asian rs8019381 frequency is much lower than European and African populations, with none of the "T" allele detected in Chinese (based on genotypes

of 90 chromosomes) and 0.006 detected in Japanese (based on genotypes of 172 chromosomes) HapMap samples. Additional studies will be necessary to identify more informative *NRXN3* rs8019381 for use in individuals with non-European heritage. Much of the evidence presented here provides an increased focus on the role of synaptic pathology in AD. Synapse losses can be documented with the first clear-cut evidence for dementia that are accompanied by synaptic toxicities conferred by *APP* [60] and *APOE* mutations [61]. The evidence in the current report suggests that A β and *APOE* synaptic pathologies are likely to interact with allele-specific alterations in gene expression of *NRXN3* transmembrane and soluble isoforms.

An astronomical number of synapses derived from about 86 billion human brain neurons [62] are dynamic

throughout the human life span, and their damage precedes neuron death due to A β oligomer (A β O) toxicity in AD [18, 63]. Substantial microscopic A β plaques are observed in old adult brains with intact cognition function [6]; however, nano-synaptic-space distribution of A β O is less known and neurexin complexes are known partners of A β [8]. Complex neurexin alternative splicing codes define synaptic specificity, strength, plasticity [15, 31], and vulnerability toward A β O [64]. The trans-synaptic anterograde and retrograde signaling of the neurexin-neuroigin-endocannabinoid system [13, 31, 65, 66] provides an attractive pathway for AD therapeutic development. Modulation of presynaptic and postsynaptic endocannabinoid tone through CB1R [67] and CB2R [68, 69], respectively, by their specific ligands might reduce neuron inflammasome and shift neurexin-neuroigin alternative splicing repertoire toward healthy synapses and reverse cognitive decline during aging [70, 71]. Neurexin peptides are significantly elevated in cerebrospinal fluid (CSF) of individuals with mild cognitive impairment (MCI), especially in patients with MCI progressing to AD dementia [72, 73]. Conceptually, targeted tryptic peptide panels of specific neurexin isoforms will improve CSF early diagnosis for pre-symptomatic AD. Screening of effective neurexin and cannabinoid receptor ligands [66, 74] and behavioral modulation of mental activities and nutrition intakes [75] might help to improve synaptic health and prevent cognitive decline 10 years or more before AD symptom appearance.

Conclusion

NRXN3 rs8019381 SNP located at SS#5 splicing site was found to contribute to AD susceptibility and interact with the *APOE* ϵ 4 haplotype. The altered expressions of *NRXN3* transmembrane and soluble isoforms were further reduced in susceptible rs8019381 heterozygous and homozygous alleles (CT or TT) in the AD postmortem cortex. The reduced *NRXN3* expression was inversely correlated with the increase of inflammasome component *NLRP3* expression in *NEUN/RBFOX3*-positive neurons in the AD brain.

Abbreviations

AD: Alzheimer's disease; A β : Amyloid beta; A β O: Amyloid beta oligomer; CSF: Cerebral spinal fluid; HIP: Hippocampus; HWE: Hardy-Weinberg equilibrium; LNS: Lamin-neurexin-sex hormone-binding globulin domains; MCI: Mild cognitive impairment; MFG: Middle frontal gyrus; MTG: Middle temporal gyrus; NFT: Neurofibrillary tangles; PCR-RFLP: PCR and restriction fragment length polymorphism; PDZ: *PSD95-Dlg1-Zo1* domain; PMI: Postmortem interval; PTM: Posttranslational modification; RT-PCR: Reverse transcription polymerase chain reaction; SNP: Single nucleotide polymorphism; SS#5: Splicing site 5

Acknowledgements

The authors acknowledge human DNA samples provided by Maryland Brain Bank (UMD) and the Collaborative Study on the Genetics of Alcoholism (COGA).

Funding

Intramural Research Programs (AG-000291-11) of NIA/NIH and the Johns Hopkins University Alzheimer's Disease Research Center (NIH P50AG05146).

Availability of data and materials

Data available on request from the author.

Authors' contributions

QRL, AH, and JME were responsible for the conception and design of the study. AH and QRL carried out the experiments and were responsible for the analysis, interpretation of the data, and drafting of the manuscript. DLL performed in the cryostat sectioning of the postmortem brain samples and RNAscope in situ hybridization. OP and JCT provided the postmortem AD and control brain samples with Braak staining stages and gave invaluable advice for the manuscript. All authors read and approved the final manuscript.

Ethics approval and consent to participate

The experiments on the postmortem brain tissues were approved by John Hopkins Medicine Institutional Review Board (https://www.hopkinsmedicine.org/institutional_review_board/index.html).

Consent for publication

Publication clearance by NIA/NIH.

Competing interests

The authors declare that they have no competing interests.

Publisher's Note

Springer Nature remains neutral with regard to jurisdictional claims in published maps and institutional affiliations.

Author details

¹Department of Psychiatry, Kobe University Graduate School of Medicine, 7-5-1 Kusunoki-Cho, Chuo-Ku, Kobe 650-0017, Japan. ²Departments of Pathology, Neuropathology Division, Johns Hopkins University School of Medicine, 600 North Wolfe Street, Baltimore, MD 21205, USA. ³Lab of Clinical Investigation, NIA-NIH, 251 Bayview Blvd, Baltimore, MD 21224, USA.

Received: 17 September 2018 Accepted: 17 February 2019

Published online: 21 March 2019

References

- Kim SH, Tang YP, Sisodia SS. Abeta star: a light onto synaptic dysfunction? *Nat Med*. 2006;12(7):760–1 discussion 761.
- Aoto J, Martinelli DC, Malenka RC, Tabuchi K, Sudhof TC. Presynaptic neurexin-3 alternative splicing trans-synaptically controls postsynaptic AMPA receptor trafficking. *Cell*. 2013;154(1):75–88.
- Coon KD, Myers AJ, Craig DW, Webster JA, Pearson JV, Lince DH, Zismann VL, Beach TG, Leung D, Bryden L, et al. A high-density whole-genome association study reveals that APOE is the major susceptibility gene for sporadic late-onset Alzheimer's disease. *J Clin Psychiatry*. 2007;68(4):613–8.
- Elman JA, Oh H, Madison CM, Baker SL, Vogel JW, Marks SM, Crowley S, O'Neil JP, Jagust WJ. Neural compensation in older people with brain amyloid-beta deposition. *Nat Neurosci*. 2014;17(10):1316–8.
- Pletnikova O, Rudow GL, Hyde TM, Kleinman JE, Ali SZ, Bharadwaj R, Gangadeen S, Crain BJ, Fowler DR, Rubio AI, et al. Alzheimer lesions in the autopsied brains of people 30 to 50 years of age. *Cogn Behav Neurol*. 2015; 28(3):144–52.
- Iacono D, Resnick SM, O'Brien R, Zonderman AB, An Y, Pletnikova O, Rudow G, Crain B, Troncoso JC. Mild cognitive impairment and asymptomatic Alzheimer disease subjects: equivalent beta-amyloid and tau loads with divergent cognitive outcomes. *J Neuropathol Exp Neurol*. 2014;73(4):295–304.
- Priller C, Bauer T, Mitteregger G, Krebs B, Kretschmar HA, Herms J. Synapse formation and function is modulated by the amyloid precursor protein. *J Neurosci*. 2006;26(27):7212–21.
- Viola KL, Velasco PT, Klein WL. Why Alzheimer's is a disease of memory: the attack on synapses by a beta oligomers (ADDLs). *J Nutr Health Aging*. 2008; 12(1):51S–7S.

9. Ushkaryov YA, Petrenko AG, Geppert M, Sudhof TC. Neurexins: synaptic cell surface proteins related to the alpha-latrotoxin receptor and laminin. *Science*. 1992;257(5066):50–6.
10. Li CY, Liu QR, Zhang PW, Li XM, Wei L, Uhl GR. OKCAM: an ontology-based, human-centered knowledgebase for cell adhesion molecules. *Nucleic Acids Res*. 2009;37(Database issue):D251–60.
11. Missler M, Sudhof TC. Neurexins: three genes and 1001 products. *Trends Genet*. 1998;14(1):20–6.
12. Sudhof TC. Neuroligins and neurexins link synaptic function to cognitive disease. *Nature*. 2008;455(7215):903–11.
13. Missler M, Zhang W, Rohlmann A, Kattenstroth G, Hammer RE, Gottmann K, Sudhof TC. Alpha-neurexins couple Ca²⁺ channels to synaptic vesicle exocytosis. *Nature*. 2003;423(6943):939–48.
14. Rudenko G. Dynamic control of synaptic adhesion and organizing molecules in synaptic plasticity. *Neural Plast*. 2017;2017:6526151.
15. Sudhof TC. Synaptic neurexin complexes: a molecular code for the logic of neural circuits. *Cell*. 2017;171(4):745–69.
16. Biederer T, Sudhof TC. Mints as adaptors. Direct binding to neurexins and recruitment of munc18. *J Biol Chem*. 2000;275(51):39803–6.
17. Hata Y, Butz S, Sudhof TC. CASK: a novel dlg/PSD95 homolog with an N-terminal calmodulin-dependent protein kinase domain identified by interaction with neurexins. *J Neurosci*. 1996;16(8):2488–94.
18. Naito Y, Tanabe Y, Lee AK, Hamel E, Takahashi H. Amyloid-beta oligomers interact with neurexin and diminish neurexin-mediated excitatory presynaptic organization. *Sci Rep*. 2017;7:42548.
19. Miller CC, McLoughlin DM, Lau KF, Tennant ME, Rogelj B. The X11 proteins, Abeta production and Alzheimer's disease. *Trends Neurosci*. 2006;29(5):280–5.
20. Hishimoto A, Liu QR, Drgon T, Pletnikova O, Walther D, Zhu XG, Troncoso JC, Uhl GR. Neurexin 3 polymorphisms are associated with alcohol dependence and altered expression of specific isoforms. *Hum Mol Genet*. 2007;16(23):2880–91.
21. Ushkaryov YA, Sudhof TC. Neurexin III alpha: extensive alternative splicing generates membrane-bound and soluble forms. *Proc Natl Acad Sci U S A*. 1993;90(14):6410–4.
22. Anderson GR, Aoto J, Tabuchi K, Foldy C, Covy J, Yee AX, Wu D, Lee SJ, Chen L, Malenka RC, et al. beta-Neurexins control neural circuits by regulating synaptic endocannabinoid signaling. *Cell*. 2015;162(3):593–606.
23. Bot N, Schweizer C, Ben Halima S, Fraering PC. Processing of the synaptic cell adhesion molecule neurexin-3beta by Alzheimer disease alpha- and gamma-secretases. *J Biol Chem*. 2011;286(4):2762–73.
24. Alarcon M, Abrahams BS, Stone JL, Duvall JA, Perederiy JV, Bomar JM, Sebat J, Wigler M, Martin CL, Ledbetter DH, et al. Linkage, association, and gene-expression analyses identify CNTNAP2 as an autism-susceptibility gene. *Am J Hum Genet*. 2008;82(1):150–9.
25. Arking DE, Cutler DJ, Brune CW, Teslovich TM, West K, Ikeda M, Rea A, Guy M, Lin S, Cook EH, et al. A common genetic variant in the neurexin superfamily member CNTNAP2 increases familial risk of autism. *Am J Hum Genet*. 2008;82(1):160–4.
26. Kim HG, Kishikawa S, Higgins AW, Seong IS, Donovan DJ, Shen Y, Lally E, Weiss LA, Najm J, Kutsche K, et al. Disruption of neurexin 1 associated with autism spectrum disorder. *Am J Hum Genet*. 2008;82(1):199–207.
27. Bierut LJ, Madden PA, Breslau N, Johnson EO, Hatsukami D, Pomerleau OF, Swan GE, Rutter J, Bertelsen S, Fox L, et al. Novel genes identified in a high-density genome wide association study for nicotine dependence. *Hum Mol Genet*. 2007;16(1):24–35.
28. Lachman HM, Fann CS, Bartzis M, Evgrafov OV, Rosenthal RN, Nunes EV, Miner C, Santana M, Gaffney J, Riddick A, et al. Genomewide suggestive linkage of opioid dependence to chromosome 14q. *Hum Mol Genet*. 2007;16(11):1327–34.
29. Kirov G, Gumus D, Chen W, Norton N, Georgieva L, Sari M, O'Donovan MC, Erdogan F, Owen MJ, Ropers HH, et al. Comparative genome hybridization suggests a role for NRXN1 and APBA2 in schizophrenia. *Hum Mol Genet*. 2008;17(3):458–65.
30. Rujescu D, Ingason A, Cichon S, Pietilainen OP, Barnes MR, Touloupoulou T, Picchioni M, Vassos E, Ettinger U, Bramon E, et al. Disruption of the neurexin 1 gene is associated with schizophrenia. *Hum Mol Genet*. 2009;18(5):988–96.
31. Aoto J, Foldy C, Ilcus SM, Tabuchi K, Sudhof TC. Distinct circuit-dependent functions of presynaptic neurexin-3 at GABAergic and glutamatergic synapses. *Nat Neurosci*. 2015;18(7):997–1007.
32. Zheng JJ, Li WX, Liu JQ, Guo YC, Wang Q, Li GH, Dai SX, Huang JF. Low expression of aging-related NRXN3 is associated with Alzheimer disease: a systematic review and meta-analysis. *Medicine (Baltimore)*. 2018;97(28):e11343.
33. Braak H, Braak E. Neuropathological staging of Alzheimer-related changes. *Acta Neuropathol*. 1991;82(4):239–59.
34. Bobinski M, de Leon MJ, Wegiel J, Desanti S, Convit A, Saint Louis LA, Rusinek H, Wisniewski HM. The histological validation of post mortem magnetic resonance imaging-determined hippocampal volume in Alzheimer's disease. *Neuroscience*. 2000;95(3):721–5.
35. Troncoso JC, Cataldo AM, Nixon RA, Barnett JL, Lee MK, Checler F, Fowler DR, Smialek JE, Crain B, Martin LJ, et al. Neuropathology of preclinical and clinical late-onset Alzheimer's disease. *Ann Neurol*. 1998;43(5):673–6.
36. Edenberg HJ, Bierut LJ, Boyce P, Cao M, Cawley S, Chiles R, Doheny KF, Hansen M, Hinrichs T, Jones K, et al. Description of the data from the Collaborative Study on the Genetics of Alcoholism (COGA) and single-nucleotide polymorphism genotyping for Genetic Analysis Workshop 14. *BMC Genet*. 2005;6(Suppl 1):S2.
37. Liu QR, Drgon T, Johnson C, Walther D, Hess J, Uhl GR. Addiction molecular genetics: 639,401 SNP whole genome association identifies many "cell adhesion" genes. *Am J Med Genet B Neuropsychiatr Genet*. 2006;141B(8):918–25.
38. Wenham PR, Price WH, Blandell G. Apolipoprotein E genotyping by one-stage PCR. *Lancet*. 1991;337(8750):1158–9.
39. Doyle ME, Fiori JL, Gonzalez Mariscal I, Liu QR, Goodstein E, Yang H, Shin YK, Santa-Cruz Calvo S, Indig FE, Egan JM. Insulin is transcribed and translated in mammalian taste bud cells. *Endocrinology*. 2018;159(9):3331–9.
40. Dupont WD, Plummer WD Jr. Power and sample size calculations for studies involving linear regression. *Control Clin Trials*. 1998;19(6):589–601.
41. Heneka MT, Kummer MP, Stutz A, Delekate A, Schwartz S, Vieira-Saecker A, Griep A, Axt D, Remus A, Tzeng TC, et al. NLRP3 is activated in Alzheimer's disease and contributes to pathology in APP/PS1 mice. *Nature*. 2013;493(7434):674–8.
42. O'Rourke NA, Weiler NC, Micheva KD, Smith SJ. Deep molecular diversity of mammalian synapses: why it matters and how to measure it. *Nat Rev Neurosci*. 2012;13(6):365–79.
43. Spiers-Jones TL, Hyman BT. The intersection of amyloid beta and tau at synapses in Alzheimer's disease. *Neuron*. 2014;82(4):756–71.
44. Kay KR, Smith C, Wright AK, Serrano-Pozo A, Pooler AM, Koffie R, Bastin ME, Bak TH, Abrahams S, Kopeikina KJ, et al. Studying synapses in human brain with array tomography and electron microscopy. *Nat Protoc*. 2013;8(7):1366–80.
45. Richter MC, Ludewig S, Winschel A, Abel T, Bold C, Salzburger LR, Klein S, Han K, Weyer SW, Fritz AK, et al. Distinct in vivo roles of secreted APP ectodomain variants APPsalpha and APPsbeta in regulation of spine density, synaptic plasticity, and cognition. *EMBO J*. 2018;37(11). <https://doi.org/10.15252/embj.201798335>.
46. Lane-Donovan C, Herz J. ApoE, ApoE receptors, and the synapse in Alzheimer's disease. *Trends Endocrinol Metab*. 2017;28(4):273–84.
47. Salazar SV, Cox TO, Lee S, Brody AH, Chyung AS, Haas LT, Strittmatter SM. Alzheimer's disease risk factor Pyk2 mediates amyloid-beta-induced synaptic dysfunction and loss. *J Neurosci*. 2019;39(4):758–72.
48. Chiocco MJ, Zhu X, Walther D, Pletnikova O, Troncoso JC, Uhl GR, Liu QR. Fine mapping of calcineurin (PPP3CA) gene reveals novel alternative splicing patterns, association of 5'UTR trinucleotide repeat with addiction vulnerability, and differential isoform expression in Alzheimer's disease. *Subst Use Misuse*. 2010;45(11):1809–26.
49. Cruchaga C, Kauwe JS, Mayo K, Spiegel N, Bertelsen S, Nowotny P, Shah AR, Abraham R, Hollingworth P, Harold D, et al. SNPs associated with cerebrospinal fluid phospho-tau levels influence rate of decline in Alzheimer's disease. *PLoS Genet*. 2010;6(9):e1001101.
50. Stallings NR, O'Neal MA, Hu J, Kavalali ET, Bezprozvanny I, Malter JS. Pin1 mediates Abeta42-induced dendritic spine loss. *Sci Signal*. 2018;11(522). <https://doi.org/10.1126/scisignal.aap8734>.
51. Levy M, Thaisz CA, Elinav E. Taming the inflammasome. *Nat Med*. 2015;21(3):213–5.
52. Supnet C, Bezprozvanny I. Neuronal calcium signaling, mitochondrial dysfunction, and Alzheimer's disease. *J Alzheimers Dis*. 2010;20(Suppl 2):S487–98.
53. Wu HY, Hudry E, Hashimoto T, Kuchibhotla K, Rozkalne A, Fan Z, Spiers-Jones T, Xie H, Arbel-Ornath M, Grosskreutz CL, et al. Amyloid beta induces the morphological neurodegenerative triad of spine loss, dendritic simplification, and neuritic dystrophies through calcineurin activation. *J Neurosci*. 2010;30(7):2636–49.
54. Holtzman DM, Morris JC, Goate AM. Alzheimer's disease: the challenge of the second century. *Sci Transl Med*. 2011;3(77):77s71.
55. Li H, Wetten S, Li L, St Jean PL, Upmanyu R, Surh L, Hosford D, Barnes MR, Briley JD, Borrie M, et al. Candidate single-nucleotide polymorphisms from

- genomewide association study of Alzheimer disease. *Arch Neurol*. 2008;65(1):45–53.
56. Reiman EM, Webster JA, Myers AJ, Hardy J, Dunckley T, Zismann VL, Joshupura KD, Pearson JV, Hu-Lince D, Huentelman MJ, et al. GAB2 alleles modify Alzheimer's risk in APOE epsilon4 carriers. *Neuron*. 2007;54(5):713–20.
 57. Bertram L, McQueen MB, Mullin K, Blacker D, Tanzi RE. Systematic meta-analyses of Alzheimer disease genetic association studies: the AlzGene database. *Nat Genet*. 2007;39(1):17–23.
 58. Chung WS, Vergheze PB, Chakraborty C, Joung J, Hyman BT, Ulrich JD, Holtzman DM, Barres BA. Novel allele-dependent role for APOE in controlling the rate of synapse pruning by astrocytes. *Proc Natl Acad Sci U S A*. 2016;113(36):10186–91.
 59. Octave JN. The amyloid peptide precursor in Alzheimer's disease. *Acta Neurol Belg*. 1995;95(4):197–209.
 60. Kero M, Paetau A, Polvikoski T, Tanskanen M, Sulkava R, Jansson L, Myllykangas L, Tienari PJ. Amyloid precursor protein (APP) A673T mutation in the elderly Finnish population. *Neurobiol Aging*. 2013;34(5):1518 e1511–1513.
 61. Terry RD. Cell death or synaptic loss in Alzheimer disease. *J Neuropathol Exp Neurol*. 2000;59(12):1118–9.
 62. Azevedo FA, Carvalho LR, Grinberg LT, Farfel JM, Ferretti RE, Leite RE, Jacob Filho W, Lent R, Herculano-Houzel S. Equal numbers of neuronal and nonneuronal cells make the human brain an isometrically scaled-up primate brain. *J Comp Neurol*. 2009;513(5):532–41.
 63. Brito-Moreira J, Lourenco MV, Oliveira MM, Ribeiro FC, Ledo JH, Diniz LP, Vital JFS, Magdesian MH, Melo HM, Barros-Aragao F, et al. Interaction of amyloid-beta (Abeta) oligomers with neurexin 2alpha and neuroligin 1 mediates synapse damage and memory loss in mice. *J Biol Chem*. 2017;292(18):7327–37.
 64. Quinn DP, Kolar A, Wigerius M, Gomm-Kolisko RN, Atwi H, Fawcett JP, Krueger SR. Pan-neurexin perturbation results in compromised synapse stability and a reduction in readily releasable synaptic vesicle pool size. *Sci Rep*. 2017;7:42920.
 65. Wang H. Endocannabinoid mediates excitatory synaptic function of beta-neurexins. Commentary: beta-neurexins control neural circuits by regulating synaptic endocannabinoid signaling. *Front Neurosci*. 2016;10:203.
 66. Schenk U, Verderio C, Benfenati F, Matteoli M. Regulated delivery of AMPA receptor subunits to the presynaptic membrane. *EMBO J*. 2003;22(3):558–68.
 67. Han X, He Y, Bi GH, Zhang HY, Song R, Liu QR, Egan JM, Gardner EL, Li J, Xi ZX. CB1 receptor activation on VgluT2-expressing glutamatergic neurons underlies delta(9)-tetrahydrocannabinol (delta(9)-THC)-induced aversive effects in mice. *Sci Rep*. 2017;7(1):12315.
 68. Liu QR, Canseco-Alba A, Zhang HY, Tagliaferro P, Chung M, Dennis E, Sanabria B, Schanz N, Escosteguy-Neto JC, Ishiguro H, et al. Cannabinoid type 2 receptors in dopamine neurons inhibits psychomotor behaviors, alters anxiety, depression and alcohol preference. *Sci Rep*. 2017;7(1):17410.
 69. Brusco A, Tagliaferro P, Saez T, Onaivi ES. Postsynaptic localization of CB2 cannabinoid receptors in the rat hippocampus. *Synapse*. 2008;62(12):944–9.
 70. Bilkei-Gorzo A, Albayram O, Draffehn A, Michel K, Piyanova A, Oppenheimer H, Dvir-Ginzberg M, Racz I, Ulas T, Imbeault S, et al. A chronic low dose of delta(9)-tetrahydrocannabinol (THC) restores cognitive function in old mice. *Nat Med*. 2017;23(6):782–7.
 71. Sarne Y, Toledano R, Rachmany L, Sasson E, Doron R. Reversal of age-related cognitive impairments in mice by an extremely low dose of tetrahydrocannabinol. *Neurobiol Aging*. 2018;61:177–86.
 72. Brinkmalm G, Sjodin S, Simonsen AH, Hasselbalch SG, Zetterberg H, Brinkmalm A, Blennow K. A parallel reaction monitoring mass spectrometric method for analysis of potential CSF biomarkers for Alzheimer's disease. *Proteomics Clin Appl*. 2018;12(1). <https://doi.org/10.1002/prca.201700131>.
 73. Duits FH, Brinkmalm G, Teunissen CE, Brinkmalm A, Scheltens P, Van der Flier WM, Zetterberg H, Blennow K. Synaptic proteins in CSF as potential novel biomarkers for prognosis in prodromal Alzheimer's disease. *Alzheimers Res Ther*. 2018;10(1):5.
 74. Sterky FH, Trotter JH, Lee SJ, Recktenwald CV, Du X, Zhou B, Zhou P, Schwenk J, Fakler B, Sudhof TC. Carbonic anhydrase-related protein CA10 is an evolutionarily conserved pan-neurexin ligand. *Proc Natl Acad Sci U S A*. 2017;114(7):E1253–62.
 75. Khalsa DS. Stress, meditation, and Alzheimer's disease prevention: where the evidence stands. *J Alzheimers Dis*. 2015;48(1):1–12.

Ready to submit your research? Choose BMC and benefit from:

- fast, convenient online submission
- thorough peer review by experienced researchers in your field
- rapid publication on acceptance
- support for research data, including large and complex data types
- gold Open Access which fosters wider collaboration and increased citations
- maximum visibility for your research: over 100M website views per year

At BMC, research is always in progress.

Learn more [biomedcentral.com/submissions](https://www.biomedcentral.com/submissions)

